

ABSOLUTE DIMENSIONS OF A FLAT HIERARCHICAL TRIPLE SYSTEM KIC 6543674 FROM THE *KEPLER* PHOTOMETRY

KENTO MASUDA^{1†}, SHO UEHARA², AND HAJIME KAWAHARA³

Draft version, June 5

ABSTRACT

Many of the *Kepler* close binaries are suggested to constitute hierarchical triple systems through their eclipse timing variations (ETVs). Eclipses by the third body in those systems, if observed, provide precise constraints on its physical and orbital properties, which are otherwise difficult to obtain. In this Letter, we analyze such a “tertiary event” observed only once in the KIC 6543674 system. The system consists of a short-period (2.4 days) inner eclipsing binary and a third body on a wide (1100 days) and eccentric ($e \simeq 0.6$) orbit. Analysis of three tertiary eclipses around a single inferior conjunction of the third body yields the mutual inclination between the inner and outer binary planes to be $3^{\circ}3 \pm 0^{\circ}6$, indicating an extremely flat geometry. Furthermore, combining the timings and shapes of the tertiary eclipses with the phase curve and ETVs of the inner binary, we determine the mass and radius ratios of all three bodies in the system using the *Kepler* photometry alone. With the primary mass and temperature from the *Kepler* Input Catalog, the absolute masses, radii, and effective temperatures of the three stars are obtained as follows: $M_A = 1.2 \pm 0.3 M_{\odot}$, $R_A = 1.8 \pm 0.1 R_{\odot}$, $M_B = 1.1^{+0.3}_{-0.2} M_{\odot}$, $R_B = 1.4 \pm 0.1 R_{\odot}$, $M_C = 0.50^{+0.07}_{-0.08} M_{\odot}$, $R_C = 0.50 \pm 0.04 R_{\odot}$, $T_A \simeq T_B \simeq 6100$ K, and $T_C < 5000$ K. Implication for the formation scenario of close binaries is briefly discussed.

Subject headings: binaries: close — binaries: eclipsing — stars: individual (KIC 6543674, KOI-5298)
— techniques: photometric

1. INTRODUCTION

Among over 2000 eclipsing binaries discovered in the *Kepler* mission (Prša et al. 2011; Slawson et al. 2011), more than 200 are suggested to host tertiary (third body) companions through their eclipse timing variations (ETVs; Conroy et al. 2014). Many of them are hierarchical triples consisting of a short-period binary and an outer third body on a wide orbit. The hierarchy is often attributed to the perturbation from the third body, as in the well-known KCTF (Kozai cycles with tidal friction) scenario (Kozai 1962; Kiseleva et al. 1998; Eggleton & Kiseleva-Eggleton 2001). Indeed, recent ETV analyses (Rappaport et al. 2013; Borkovits et al. 2015) have revealed many hierarchical triples with misaligned tertiary orbits, whose mutual inclinations exhibit suggestive peaks around $\sim 40^{\circ}$ in agreement with the KCTF prediction (Fabrycky & Tremaine 2007).

On the other hand, at least 10 or more hierarchical triples seem to have well-aligned orbits, as suggested by eclipses due to tertiary companions (Carter et al. 2011; Orosz 2015, figure 7). Three-dimensional geometry and absolute dimensions of those systems are also of interest because their hierarchy may argue for the mechanism of orbital shrinkage that do not require high mutual inclinations between the inner and outer binary planes (e.g., Petrovich 2015).

In this Letter, we focus on a tertiary event observed only once in the KIC 6543674 system, which involves three tertiary eclipses around a single inferior conjunction of the third body (Figure 1). Although this event has already been reported (Slawson et al. 2011; Thackeray-Lacko et al. 2013; Conroy et al. 2014), the information obtained from its detailed modeling has not yet been clarified. Below we will show that the tertiary event plays two crucial roles in determining the system configuration. First, it constrains the mutual inclination between the inner and outer binary orbits very precisely, in a similar way to the “planet–planet eclipse” known in the *Kepler* multi-transiting planetary system(s) (Hirano et al. 2012; Masuda et al. 2013; Masuda 2014). Secondly, and less trivially, it fixes the mass ratio of the inner binary and velocity of the third body even without spectroscopy.

The present Letter reports precise geometry and absolute dimensions of the KIC 6543674 system. We combine the above information from the tertiary event with the complementary constraints from ETVs and eclipses of the inner binary. To obtain a consistent solution, we fit the three components simultaneously using a Markov Chain Monte Carlo (MCMC) method. Section 2 presents individual analyses of the ETVs and eclipse curves of the inner binary. We then model the two components jointly with the tertiary eclipses in Section 3 to determine the parameters of the whole system. Section 4 discusses the implication of the resulting system architecture and the prospects for the follow-up observations to better understand this valuable system.

† masuda@utap.phys.s.u-tokyo.ac.jp

¹ Department of Physics, The University of Tokyo, Tokyo 113-0033, Japan

² Department of Physics, Tokyo Metropolitan University, Tokyo 192-0397, Japan

³ Department of Earth and Planetary Science, The University of Tokyo, Tokyo 113-0033, Japan

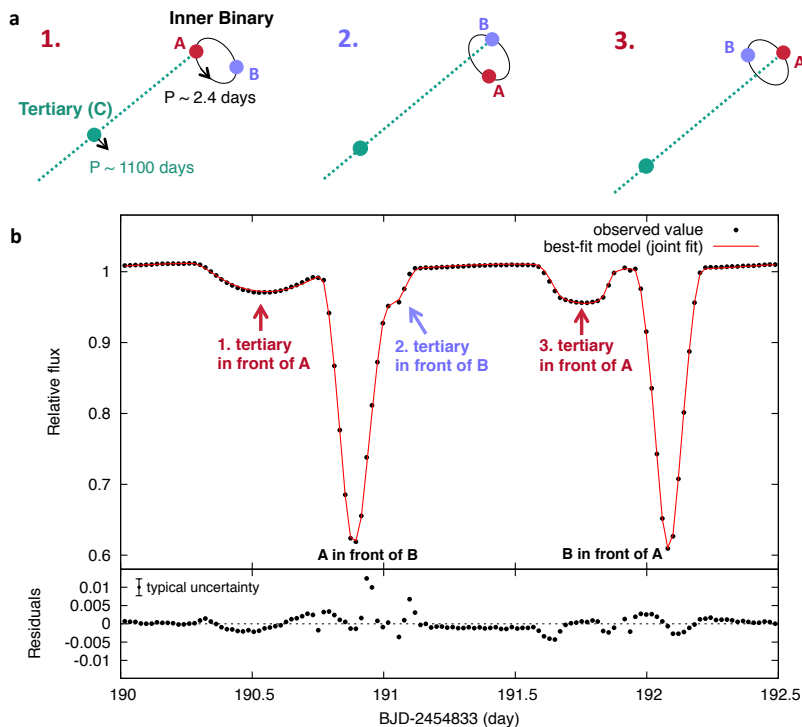


FIG. 1.— Tertiary event observed in the KIC 6543674 system and its interpretation. (a) Schematic illustration of the system configuration during the event. (b) Fit to the *Kepler* light curve around the tertiary eclipses (see Section 3). (*Top*) Black circles are the observed fluxes and red solid line denotes our best-fit model. (*Bottom*) Residuals of our fit. Typical uncertainty estimated from our analysis ($\simeq \sigma_{\text{LC, tertiary}}$) is shown at the upper left.

2. CONSTRAINTS FROM ETVs AND PHASE CURVE OF THE INNER BINARY

The KIC 6543674 system consists of the inner eclipsing binary with the orbital period of $P_{\text{in}} \simeq 2.39$ days and the “outer” eccentric binary (third body moving around the center of mass of the inner binary) with $P_{\text{out}} \simeq 1100$ days. Here we present individual MCMC analyses of the phase curve and ETVs of the inner binary, which allow us to constrain the orbital geometries of the inner and outer binaries, respectively. Since $P_{\text{in}}/P_{\text{out}}$ is small, both inner and outer binary orbits are approximately Keplerian. We adopt the approximation throughout the paper and define all the orbital elements in Jacobi coordinates (with subscripts “in” and “out”), which are in this case constant over time.

2.1. ETV Analysis

The inner binary exhibit ETVs, which were used to infer the existence of the third body (Conroy et al. 2014). They are caused by the finite light-travel time (Rømer delay) and the variation in the line-of-sight distance due to the outer binary motion. Under our assumption, the i th eclipse time of the inner binary t_i can be modeled as (Rappaport et al. 2013)⁴

$$t_i^{\text{model}} = t_{0,\text{in}} + P_{\text{in}}i + A_{\text{ETV}} \left\{ \sqrt{1 - e_{\text{out}}^2} \sin E_{\text{out}}(t_i) \cos \omega_{\text{out}} + [\cos E_{\text{out}}(t_i) - e_{\text{out}}] \sin \omega_{\text{out}} \right\}. \quad (1)$$

Here, $t_{0,\text{in}}$ is the eclipse epoch (time of inferior conjunction) of the inner binary, and e_{out} , ω_{out} , and E_{out} are the eccentricity, argument of pericenter, and eccentric anomaly of the third body. The amplitude of ETVs, A_{ETV} , is given by the projected semi-major axis of the outer binary $a_{\text{out}} \sin i_{\text{out}}$ divided by the speed of light c :

$$A_{\text{ETV}} = \frac{(GM_A)^{1/3}}{c(2\pi)^{2/3}} \frac{(M_C/M_A) \sin i_{\text{out}}}{(1 + M_B/M_A + M_C/M_A)^{2/3}} P_{\text{out}}^{2/3}, \quad (2)$$

where M denotes the stellar mass, with the subscripts A , B , and C specifying the primary, secondary, and tertiary stars, respectively. In such a hierarchical system as KIC 6543674, dynamical effects that change P_{in} are sufficiently smaller than the above effect and so are neglected (Rappaport et al. 2013).

We use Equation (1) to model the primary eclipse times t_i^{obs} in table 1 of Conroy et al. (2014) obtained by fitting the light curve over the entire phase (flagged as “entire”). The observed ETVs also exhibit short-term modulations (see Figure 2a), which can be explained by star spots if the stellar rotation is nearly (but not exactly) synchronized

⁴ The sign is opposite to their equation (6) because we take $+z$ -axis in the observer’s direction.

TABLE 1
 SYSTEM PARAMETERS FROM THE *Kepler* LIGHT CURVES.

Parameter	ETVs	phase curve	ETVs + phase + tertiary	ETVs + phase + tertiary (with the prior on M_A from KIC)
<i>(Inner binary)</i>				
$t_{0,\text{in}}$ (BJD - 2454833)	132.3070 ± 0.0002	...	132.3071 ± 0.0001	132.30704 ± 0.00009
$t_{0,\text{in}}^{\text{phase}}$ (BJD - 2454833)	...	132.30372 ± 0.00004	132.30372 ± 0.00003	$132.30372^{+0.00002}_{-0.00003}$
P_{in} (day)	2.3910305 ± 0.0000003	2.3910305 (fixed)	2.3910305 ± 0.0000003	2.3910305 ± 0.0000002
a_{in}/R_A	...	5.49 ± 0.02	$5.494^{+0.007}_{-0.006}$	$5.494^{+0.006}_{-0.007}$
$\cos i_{\text{in}}$...	0.021 ± 0.002	0.022 ± 0.002	0.022 ± 0.002
$e_{\text{in}} \cos \omega_{\text{in}}$...	$(0.2 \pm 3.3) \times 10^{-5}$	0 (fixed)	0 (fixed)
$e_{\text{in}} \sin \omega_{\text{in}}$...	$-0.0005^{+0.0021}_{-0.0020}$	0 (fixed)	0 (fixed)
R_B/R_A	...	0.781 ± 0.004	0.781 ± 0.002	0.781 ± 0.002
M_B/M_A	0.93 ± 0.02	0.93 ± 0.02
C_{phase}	...	1.00259 ± 0.00002	1.00259 ± 0.00002	1.00259 ± 0.00002
T_B/T_A	...	1.012 ± 0.002	1.0107 ± 0.0004	1.0107 ± 0.0004
u_A	...	0.45 ± 0.04	0.434 ± 0.009	0.434 ± 0.009
u_B	...	0.46 ± 0.03	0.47 ± 0.02	0.46 ± 0.02
A_0	...	0.041 ± 0.007	0.037 ± 0.006	0.037 ± 0.006
A_{1c}	...	0.00034 ± 0.00005	0.00035 ± 0.00005	0.00035 ± 0.00005
A_{1s}	...	0.00096 ± 0.00004	0.00096 ± 0.00004	0.00096 ± 0.00004
A_{2c}	...	-0.00720 ± 0.00007	-0.00716 ± 0.00006	-0.00716 ± 0.00006
$R_A (R_{\odot})$	$2.1^{+3.2}_{-0.3} \dagger$	$1.8 \pm 0.1 \dagger$
$R_B (R_{\odot})$	$1.6^{+2.5}_{-0.7} \dagger$	$1.4 \pm 0.1 \dagger$
$M_A (M_{\odot})$	$1.8^{+27.5}_{-1.4} \dagger$	1.2 ± 0.3
$M_B (M_{\odot})$	$1.7^{+25.5}_{-1.3} \dagger$	$1.1^{+0.3}_{-0.2} \dagger$
<i>(Third body)</i>				
$t_{0,\text{out}}$ (BJD - 2454833)	199 ± 10	...	191.246 ± 0.003	191.246 ± 0.003
P_{out} (day)	1086^{+8}_{-7}	...	1090 ± 6	1090 ± 5
$e_{\text{out}} \cos \omega_{\text{out}}$	0.13 ± 0.05	...	0.16 ± 0.03	0.16 ± 0.03
$e_{\text{out}} \sin \omega_{\text{out}}$	0.58 ± 0.03	...	0.58 ± 0.02	0.572 ± 0.008
a_{out}/R_A	345^{+15}_{-13}	$348 \pm 2 \dagger$
$\cos i_{\text{out}}$	0.0030 ± 0.0003	$0.0029^{+0.0001}_{-0.0002}$
$\Delta\Omega$ (deg)	3.2 ± 0.6	3.1 ± 0.6
A_{ETV} (s)	264 ± 6	...	266 ± 5	$265 \pm 5 \dagger$
C_{tertiary}	1.0070 ± 0.0003	1.0070 ± 0.0003
γ_{tertiary} (day^{-1})	0.00004 ± 0.00021	$0.00005^{+0.00021}_{-0.00022}$
R_C/R_A	0.277 ± 0.003	0.277 ± 0.003
M_C/M_A	$0.4^{+0.3}_{-0.2} \dagger$	$0.43^{+0.04}_{-0.03}$
T_C/T_A	$0.84^{+0.03}_{-0.04} \dagger$	$0.84^{+0.03}_{-0.04} \dagger$
$R_C (R_{\odot})$	$0.6^{+0.9}_{-0.2} \dagger$	$0.50 \pm 0.04 \dagger$
$M_C (M_{\odot})$	$0.7^{+3.3}_{-0.4} \dagger$	$0.50^{+0.07}_{-0.08} \dagger$
mutual inclination (deg)	$3.3 \pm 0.6 \dagger$	$3.3^{+0.3}_{-0.6} \dagger$
<i>(Jitters)</i>				
σ_{ETV} (s)	56 ± 3	...	56 ± 3	56 ± 3
$\sigma_{\text{LC,phase}}$...	0.00048 ± 0.00001	0.00049 ± 0.00001	0.00049 ± 0.00001
$\sigma_{\text{LC,tertiary}}$	0.0023 ± 0.0002	$0.0023^{+0.0002}_{-0.0001}$

NOTE. — The quoted values and uncertainties are the median and 68.3% credible interval of the marginalized posteriors. Values marked with daggers are derived from the posteriors of other fitted parameters.

with the inner binary motion (see, e.g., figure 3 of Orosz 2015). Instead of modeling them, we include an additional scatter σ_{ETV} to the formal eclipse-time error σ_i in quadrature to define the following likelihood for the ETV fit:

$$\mathcal{L}_{\text{ETV}} = \prod_i \frac{1}{\sqrt{2\pi(\sigma_i^2 + \sigma_{\text{ETV}}^2)}} \exp \left[-\frac{(t_i^{\text{obs}} - t_i^{\text{model}})^2}{2(\sigma_i^2 + \sigma_{\text{ETV}}^2)} \right]. \quad (3)$$

This likelihood is used to perform an MCMC sampling (emcee by Foreman-Mackey et al. 2013) of the posteriors of the parameters in the second column of Table 1. The best-fit model is compared with the observed values in Figure 2a.

2.2. Phase-Curve Analysis

The linear ephemeris of the inner binary ($t_{0,\text{in}}$ and P_{in}) obtained in Section 2.1 is used to phase-fold the light curve taken from the *Kepler* eclipsing binary catalog,⁵ whose instrumental trend has been removed (“flattened”) using polynomials (Conroy et al. 2014). Since A_{ETV} is shorter than the data cadence (29.4 minutes), we do not correct for ETVs here and in the following light-curve fitting (Section 3). The folded fluxes are averaged into three minute bins,

⁵ <http://keplerebs.villanova.edu>

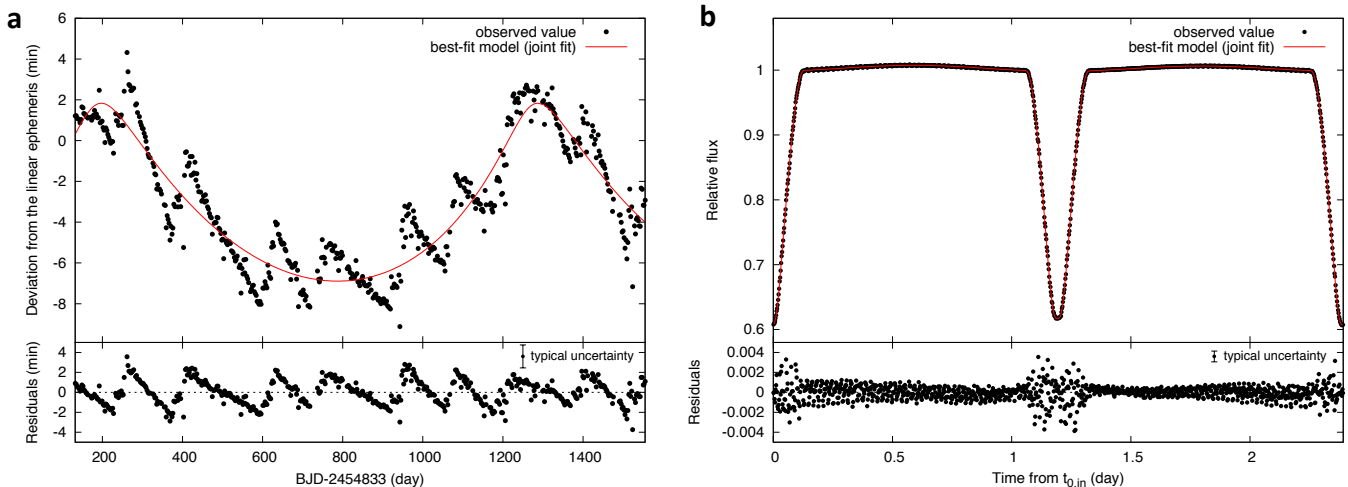


FIG. 2.— (a) Fit to the eclipse times. (*Top*) Black circles are the observed eclipse times and red solid line denotes our best-fit model. Only the deviations from the linear ephemeris are shown for clarity. (*Bottom*) Residuals of our fit. Typical (jitter-included) uncertainty is shown at the upper right. (b) Fit to the folded phase curve. (*Top*) Black circles are the observed fluxes and red solid line denotes our best-fit model. (*Bottom*) Same as panel (a).

and the flux value and error in each bin are estimated as the median and 1.4826 times median absolute deviation divided by the square root of the number of points in the bin.

We model the flux over the entire phase as

$$f_{\text{phase}}(t) = \frac{C_{\text{phase}}}{1 + F_B/F_A + A_0} \left[f_A(t) + \frac{F_B}{F_A} f_B(t) + A_0 + A_{1c} \cos \phi + A_{1s} \sin \phi + A_{2c} \cos 2\phi \right]. \quad (4)$$

Here, $f_{A,B}(t)$ is the normalized stellar flux computed with the analytic eclipse model by Mandel & Agol (2002) for the linear limb darkening law. They are determined from the orbital ephemeris, scaled semi-major axis a_{in}/R_A , cosine of the orbital inclination $\cos i_{\text{in}}$, radius ratio R_B/R_A , and linear limb-darkening coefficients u_A and u_B . The flux ratio, F_B/F_A , is computed by $(R_B/R_A)^2(T_B/T_A)^4$, where T is the stellar effective temperature in the *Kepler* band. The constants A_0 , A_{1c} , A_{1s} , and A_{2c} are the phenomenological parameters to describe the phase-curve modulation, and $\phi = 2\pi(t - t_{0,\text{in}})/P_{\text{in}}$ is the orbital phase.⁶ These amplitudes, in principle, can be related to the masses of the two bodies with the physical model of ellipsoidal variation and Doppler beaming (Morris & Naftilan 1993; Loeb & Gaudi 2003). We do not use them for the mass estimates, however, because our quarter-by-quarter analysis reveals the temporal variation in the shape of the phase curve. This variation is also consistent with the star-spot modulation nearly synchronized with the orbital motion. Finally, C_{phase} is the overall normalization. In fitting the observed data, $f_{\text{phase}}(t)$ is averaged over 30 minutes around each time to take into account the long-cadence sampling. The light-travel time effect is neglected in computing $f_{\text{phase}}(t)$ because it is shorter than the data cadence.

As in Section 2.1, we use an MCMC algorithm to fit the phase-folded light curve for the above parameters. We again include the “jitter” term $\sigma_{\text{LC,phase}}$ in the likelihood $\mathcal{L}_{\text{phase}}$ defined in the same way as in Equation (3). The resulting constraints are in the third column of Table 1, and the best-fit light curve is shown in Figure 2b. We also try floating e_{in} and ω_{in} , only to find that the inner orbit is very close to circular. Hence we fix $e_{\text{in}} = 0$ in the following analyses.

The residuals in the bottom panel of Figure 2b exhibit an out-of-eclipse warp and a larger in-eclipse scatter (similar to the one in Bass et al. 2012). The former does not affect our analysis significantly because we do not extract any physical information from the out-of-eclipse modulation. On the other hand, the latter points to systematics that affect the shape of eclipses and thus may bias the resulting system parameters. While it may be due to the spot occultation, ETVs we neglected could also affect the eclipse signal by a similar amount ($A_{\text{ETV}}/(\text{ingress duration}) \sim \mathcal{O}(1\%)$). Although unlikely to explain the random scatter, we also note that the Mandel & Agol (2002) model is exact only for spherical stars and so neglects the tidal distortion of $\mathcal{O}(1\%)$ suggested by the value of A_{2c} . In any case, the results of the following analyses could suffer from that level of systematics, though the main conclusions remain unchanged.

3. GEOMETRY AND ABSOLUTE DIMENSIONS FROM THE TERTIARY EVENT

In this section, we analyze the light curve of the tertiary event jointly with the two components in the previous section. The outer binary motion of the third body is converted to the motions relative to the primary and secondary, which are used to compute their normalized fluxes including the tertiary eclipses, $f_{A,\text{tertiary}}(t)$ and $f_{B,\text{tertiary}}(t)$, with the Mandel & Agol (2002) model. This requires a_{out}/R_A , $\cos i_{\text{out}}$, R_C/R_A , $\Delta\Omega$ (difference in the longitudes of ascending node between inner and outer orbits) and M_B/M_A in addition to the parameters in Section 2. They are incorporated

⁶ Since ETVs we neglected may shift the center of the phase curve, we allow $t_{0,\text{in}}$ used for the phase-curve fitting (denoted as $t_{0,\text{in}}^{\text{phase}}$) to be different from $t_{0,\text{in}}$ in Equation (1). The resulting difference ($|t_{0,\text{in}}^{\text{phase}} - t_{0,\text{in}}| \simeq 5$ minutes) is actually comparable to A_{ETV} and consistent with the ETV origin.

in the model flux during the tertiary event as

$$f_{\text{tertiary}}(t) = \frac{C_{\text{tertiary}} + \gamma_{\text{tertiary}}(t - t_*)}{1 + F_{\text{B}}/F_{\text{A}} + A_0} \left[f_{\text{A,tertiary}}(t) + \frac{F_{\text{B}}}{F_{\text{A}}} f_{\text{B,tertiary}}(t) + A_0 + A_{1c} \cos \phi + A_{1s} \sin \phi + A_{2c} \cos 2\phi \right], \quad (5)$$

where C_{tertiary} is the normalization, γ_{tertiary} models the residual instrumental trend around the tertiary event, and we choose $t_*(\text{BJD} - 2454833) = 191.25$. The model likelihood for the tertiary-event light curve $\mathcal{L}_{\text{tertiary}}$ is defined in the same way as in $\mathcal{L}_{\text{phase}}$, again including an additional jitter $\sigma_{\text{LC,tertiary}}$. We first seek for the solution that maximizes $\mathcal{L}_{\text{tertiary}}$ with $\sigma_{\text{LC,tertiary}} = 0$ for various $t_{0,\text{out}}$ using the Levenberg-Marquardt method (Markwardt 2009). Here the above seven new parameters are fitted, while the others are floated within the 3σ boundaries from the ETVs and phase curve (Table 1). We then perform an MCMC run from the solution, fitting all the model parameters simultaneously with the joint likelihood $\mathcal{L} \propto \mathcal{L}_{\text{ETV}} \cdot \mathcal{L}_{\text{phase}} \cdot \mathcal{L}_{\text{tertiary}}$. The resulting constraints are summarized in the fourth column of Table 1 along with other derived parameters. As shown in Figure 1, our model well reproduces the observed tertiary eclipses. In the following subsections, we discuss the information newly derived from the tertiary eclipses.

3.1. Mutual Inclination

Tertiary eclipses on both of the inner two stars suggest a well-alignment between inner and outer binary planes. This naive expectation is quantified by our modeling. We obtain $i_{\text{out}} = 89^\circ 83 \pm 0^\circ 02$ and $\Delta\Omega = 3^\circ 2 \pm 0^\circ 6$ (see Figure 3b) as the line-of-sight and sky-plane inclinations of the tertiary orbit. Combined with $i_{\text{in}} = 88^\circ 7 \pm 0^\circ 1$, these results indicate an extremely flat orbital configuration, with the 3σ upper limit on the mutual inclination being 5° .

3.2. Relative Dimensions

Another role of the tertiary event is to determine the mass ratio $M_{\text{B}}/M_{\text{A}}$ and the tertiary-to-primary velocity ratio $V_{\text{C}}/V_{\text{A}}$ during the event, where V is the orbital velocity relative to the center of mass of the inner binary. The constraints are invaluable because they allow us to determine the mass ratios of all three bodies. It is even possible, in principle, to combine them with the ETV amplitude to fix the absolute dimensions of the whole system from photometry alone.

The two quantities, $M_{\text{B}}/M_{\text{A}}$ and $V_{\text{C}}/V_{\text{A}}$, are closely related to the timings and durations of the three tertiary eclipses. The bottom panel of Figure 3a shows the approximately one-dimensional motion of the inner binary in the sky plane with respect to its center of mass (red and blue sinusoidal lines). Here the motion of the third body (green line) is represented by an almost straight line owing to its long orbital period. For $\Delta\Omega \simeq 0^\circ$, eclipses occur at the intersections of the two lines in this diagram. Thus, the green line should cross either of the red or blue sinusoids at the times of three tertiary eclipses (vertical dashed lines), roughly within the primary/secondary radii (vertical error bars). The condition essentially fixes the amplitude of the blue sinusoid and the slope of the green line, which correspond to $M_{\text{A}}/M_{\text{B}}$ and $V_{\text{C}}/V_{\text{A}}$, respectively. The ratio $V_{\text{C}}/V_{\text{A}}$ is further constrained by the relative durations of the first and third tertiary eclipses, where the relative velocities between the two stars are $V_{\text{A}} - V_{\text{C}}$ and $V_{\text{A}} + V_{\text{C}}$, respectively.

These ratios yield the relative mass of the third body as well. Using P_{in} , $a_{\text{in}}/R_{\text{A}}$, $t_{0,\text{out}}$, P_{out} , e_{out} , and ω_{out} we already derived, $V_{\text{C}}/V_{\text{A}}$ is converted to $a_{\text{out}}/R_{\text{A}}$. Since this a_{out} should satisfy Kepler's third law, we obtain

$$\left(\frac{a_{\text{out}}/R_{\text{A}}}{a_{\text{in}}/R_{\text{A}}} \right)^3 \left(\frac{P_{\text{in}}}{P_{\text{out}}} \right)^2 = 1 + \frac{M_{\text{C}}/M_{\text{A}}}{1 + M_{\text{B}}/M_{\text{A}}}, \quad (6)$$

which can be solved for $M_{\text{C}}/M_{\text{A}}$ as

$$\frac{M_{\text{C}}}{M_{\text{A}}} = \left[\left(\frac{a_{\text{out}}/R_{\text{A}}}{a_{\text{in}}/R_{\text{A}}} \right)^3 \left(\frac{P_{\text{in}}}{P_{\text{out}}} \right)^2 - 1 \right] \left(1 + \frac{M_{\text{B}}}{M_{\text{A}}} \right). \quad (7)$$

The mass ratios derived in this way are listed in Table 1. These values indicate that the system is dynamically stable, according to the criterion by Mardling & Aarseth (2001).

In fact, the timings of the three eclipses alone allow for other configurations, though they do not fit the eclipse shapes well and hence are rejected (Figure 4).⁷ Those in panels (c) and (d) yield too short durations for the third eclipse due to the head-on crossing with one of the inner binary. Moreover, the solutions are unphysical because the values of $a_{\text{out}}/R_{\text{A}}$ are so small that $M_{\text{C}}/M_{\text{A}} < 0$ is required in Equation (6). The solution in panel (b), which is the retrograde version of the best solution, fits the light curve better than those in (c) and (d); however, large residuals remain around the first and third tertiary eclipses because R_{B} is slightly smaller than R_{A} .

Similarly to $F_{\text{B}}/F_{\text{A}}$, the constant A_0 could also be related to the third-body temperature by $T_{\text{C}}/T_{\text{A}} = A_0^{1/4} (R_{\text{C}}/R_{\text{A}})^{-1/2}$, which is also listed in Table 1. The value of $T_{\text{C}}/T_{\text{A}}$ thus determined, however, should be considered as a rough upper limit because A_0 includes contaminations from nearby sources and/or systematics in the phase-curve modulation.

⁷ Since these solutions include different $M_{\text{B}}/M_{\text{A}}$, a radial velocity follow-up is also useful to confirm our solution independently of the possible systematics discussed in Section 2.2.

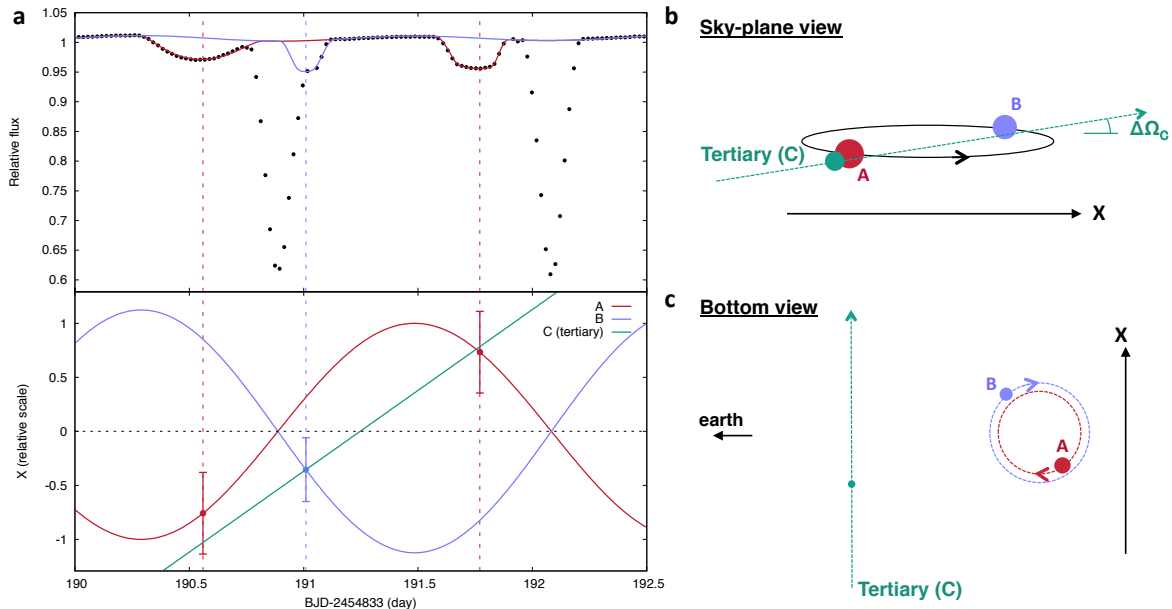


FIG. 3.— (a) Relationship between the timings of three tertiary eclipses and motions of three stars. (*Top*) The black dots denote the detrended *Kepler* light curve. The red and blue lines are the best-fit tertiary eclipse models for stars A and B, respectively. The vertical dashed lines denote the rough central times of the tertiary eclipses. (*Bottom*) One-dimensional motion of the three stars (primary: red, secondary: blue, tertiary: green) with respect to the center of mass of the inner binary. The X -axis is defined to coincide with the line of nodes of the inner binary, with its positive direction shown in panels (b) and (c). The amplitude of the primary motion is normalized to unity, while that of the secondary depends on M_B/M_A (notice that only the relative scale affects the light curve). The vertical bars denote the normalized radii of stars A (red) and B (blue). (b) Sky-plane view and (c) bottom view of the system. Definitions of $\Delta\Omega$ and X -axis are shown schematically.

3.3. Absolute Dimensions

Combined with the ETV amplitude in Equation (2), the mass ratios above can be further used to determine the absolute masses of the system as

$$M_A = 1.074 \times 10^{-3} M_\odot \left(\frac{A_{\text{ETV}}}{s} \right)^3 \left(\frac{P_{\text{out}}}{\text{day}} \right)^{-2} \frac{(1 + M_B/M_A + M_C/M_A)^2}{(M_C/M_A)^3 \sin^3 i_{\text{out}}}. \quad (8)$$

Correspondingly, absolute radii are obtained from $a_{\text{in}} = [P_{\text{in}}^2 G M_A (1 + M_B/M_A) / 4\pi^2]^{1/3}$ and a_{in}/R_A . The constraints on the absolute dimensions, however, are very weak (see Table 1) due to the strong correlation $M_A \sim (M_C/M_A)^{-3} \sim (a_{\text{out}}/R_A)^{-9}$ as implied by Equations (7) and (8).

The constraints are significantly improved with a better constraint on either M_A or M_C/M_A . To demonstrate this, we repeat the above joint analysis with the Gaussian prior on the primary mass $M_A = 1.15 \pm 0.28 M_\odot$ based on the value in the *Kepler* Input Catalog (KIC). Here M_A and M_C/M_A are chosen to be fitting parameters instead of a_{out}/R_A and A_{ETV} , where the former two are converted to the latter using Equations (2) and (6). The results are summarized in the last column of Table 1. While the constraints on the geometry and relative dimensions are almost unchanged, the absolute masses and radii of all three stars are now determined to the precision similar to the prior constraint. If we also adopt the KIC effective temperature for the primary, we obtain $T_A = T_B = 6100 \pm 200$ K and $T_C < 5000$ K. The dimensions are consistent with the Dartmouth isochrone (Dotter et al. 2008) of ~ 7 -8 Gyr and suggest that the inner two stars have entered the subgiant branch and that the third body is an M dwarf (Lépine et al. 2013), though the conclusion is sensitive to the priors on M_A and T_A .

4. DISCUSSION

In this Letter, we determine the geometry and physical properties of the hierarchical triple system KIC 6543674 using the *Kepler* photometry alone. Especially, the tertiary event analyzed here enables us to obtain (i) mutual inclination between the inner and outer binary planes, and (ii) mass ratio of the inner binary and instantaneous orbital velocity of the third body. Our analysis clarifies the value of the tertiary eclipses in hierarchical systems with the clear and textbook-like example of the event. The methodology presented here is basically applicable to other hierarchical systems involving tertiary eclipses on both of the inner stars, though more sophisticated models of the eclipse light curve and/or ETVs may be required to accurately model those systems with smaller P_{in} and/or $P_{\text{out}}/P_{\text{in}}$. Here it is worth noting that the KIC 6543674 system has the longest P_{out} among the known triply eclipsing hierarchical triples.

The flatness of the system we find (within a few degrees) may have interesting implications for the the origin of the closest binaries, though it is not clear at this point how it compares to the large sample of misaligned triples (Rappaport et al. 2013; Borkovits et al. 2015) as predicted by the KCTF scenario. In this context, a large eccentricity of the third body is intriguing because it may argue for the excitation of the inner orbit's eccentricity on the octupole

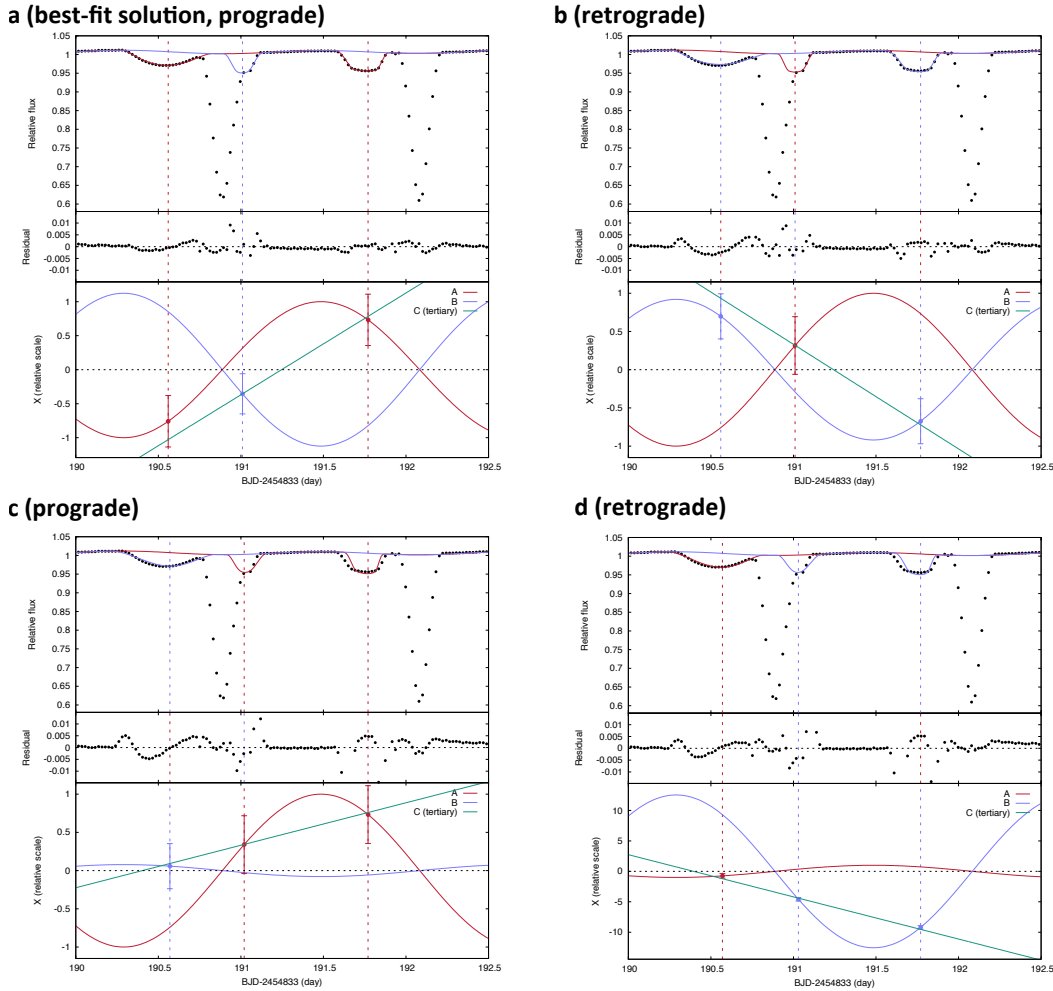


FIG. 4.— Comparison between the best-fit solution (panel a) and other solutions allowed from the timings of the three eclipses alone (panels b, c, and d). The meaning of each panel is basically the same as Figure 3a, but this time the residuals for each solution is shown in the middle using the same scales.

order (e.g., Li et al. 2014; Petrovich 2015). In any case, the relative/absolute dimensions of the system as constrained here will be useful for testing those possible alternatives.

Although the absolute dimensions derived above are based on the KIC value, which is of limited reliability, they can be made more accurate with the follow-up spectroscopy to better constrain the stellar photospheric parameters and/or to measure radial velocities, even if they only cover the inner binary orbit. In addition, follow-up photometry of another tertiary event will pin down P_{out} far more precisely, and can also give us some insight into the dynamical interaction in the system. In fact, the non-detection of the second tertiary event in the *Kepler* data, which would have occurred around $\text{BJD} = 2456114 \pm 5$ from our result, suggests that the actual period is $\sim 2\sigma$ longer than our estimate and that the second event was hidden in the data gap of about 6 days centered around $\text{BJD} = 2456126$. The fact also motivates the ground-based observation of the next event, which would be around July in 2015.

We are grateful to the entire *Kepler* team for their revolutionary data; Takayuki Kotani and Shin'ya Yamada for fruitful discussions; and an anonymous referee for many helpful suggestions. This work is supported by JSPS Grant-in-Aid for Scientific Research No. 26-7182 (K.M.) and 25800106 (H.K.) and by Research Center for the Early Universe (RESCEU). K.M. is also supported by the Leading Graduate Course for Frontiers of Mathematical Sciences and Physics.

REFERENCES

- Bass, G., Orosz, J. A., Welsh, W. F., et al. 2012, *ApJ*, 761, 157
 Borkovits, T., Rappaport, S., Hajdu, T., & Sztakovics, J. 2015, *MNRAS*, 448, 946
 Carter, J. A., Fabrycky, D. C., Ragozzine, D., et al. 2011, *Science*, 331, 562
 Conroy, K. E., Prša, A., Stassun, K. G., et al. 2014, *AJ*, 147, 45
 Dotter, A., Chaboyer, B., Jevremović, D., et al. 2008, *ApJS*, 178, 89
 Eggleton, P. P., & Kiseleva-Eggleton, L. 2001, *ApJ*, 562, 1012
 Fabrycky, D., & Tremaine, S. 2007, *ApJ*, 669, 1298
 Foreman-Mackey, D., Hogg, D. W., Lang, D., & Goodman, J. 2013, *PASP*, 125, 306
 Hirano, T., Narita, N., Sato, B., et al. 2012, *ApJ*, 759, L36

- Kiseleva, L. G., Eggleton, P. P., & Mikkola, S. 1998, *MNRAS*, 300, 292
- Kozai, Y. 1962, *AJ*, 67, 591
- Lépine, S., Hilton, E. J., Mann, A. W., et al. 2013, *AJ*, 145, 102
- Li, G., Naoz, S., Kocsis, B., & Loeb, A. 2014, *ApJ*, 785, 116
- Loeb, A., & Gaudi, B. S. 2003, *ApJ*, 588, L117
- Mandel, K., & Agol, E. 2002, *ApJ*, 580, L171
- Mardling, R. A., & Aarseth, S. J. 2001, *MNRAS*, 321, 398
- Markwardt, C. B. 2009, in *Astronomical Society of the Pacific Conference Series*, Vol. 411, *Astronomical Data Analysis Software and Systems XVIII*, ed. D. A. Bohlender, D. Durand, & P. Dowler, 251
- Masuda, K. 2014, *ApJ*, 783, 53
- Masuda, K., Hirano, T., Taruya, A., Nagasawa, M., & Suto, Y. 2013, *ApJ*, 778, 185
- Morris, S. L., & Naftilan, S. A. 1993, *ApJ*, 419, 344
- Orosz, J. A. 2015, *ArXiv e-prints*, arXiv:1503.07295
- Petrovich, C. 2015, *ApJ*, 805, 75
- Prša, A., Batalha, N., Slawson, R. W., et al. 2011, *AJ*, 141, 83
- Rappaport, S., Deck, K., Levine, A., et al. 2013, *ApJ*, 768, 33
- Slawson, R. W., Prša, A., Welsh, W. F., et al. 2011, *AJ*, 142, 160
- Thackeray-Lacko, B., Hill, M., Orosz, J. A., et al. 2013, in *American Astronomical Society Meeting Abstracts*, Vol. 221, *American Astronomical Society Meeting Abstracts* 221, 142.09